Check for updates

Xe···OCS: relatively straightforward?†‡

Peter Kraus, [ID] §*[a] Daniel A. Obenchain, [ID] §[b] Sven Herbers, [ID] [b]
Dennis Wachsmuth,[b] Irmgard Frank[a] and Jens-Uwe Grabow [ID] [b]

We report a benchmark-quality equilibrium-like structure of the Xe···OCS complex, obtained from microwave spectroscopy. The experiments are supported by a wide array of highly accurate calculations, expanding the analysis to the complexes of He, Ne, Ar, Kr, Xe, and Hg with OCS. We investigate the trends in the structures and binding energies of the complexes. The assumption that the structure of the monomers does not change significantly upon forming a weakly bound complex is also tested. An attempt at reproducing the $r_m^{(2)}$ structure of the Xe···OCS complex with correlated wavefunction theory is made, highlighting the importance of relativistic effects, large basis sets, and inclusion of diffuse functions in extrapolation recipes.

1 Introduction

Nicolas Cage once said that "every great story seems to begin with a snake." Our story began with the COBRA microwave spectrometer¶ undergoing maintenance, after which we've decided to check the instrument by recording a spectrum of carbonyl sulphide (OCS). In the field of microwave spectroscopy, OCS is probably the most often intentionally studied gas. Every rotational spectroscopy lab has buckets of this stinky stuff: it is not particularly expensive, it has been well characterised since the 60's,[1] it has a well-defined spectrum with easily populated transitions, a precise value of its dipole moment is known,[2] and it is stable. Therefore, it is quite useful for setting up instruments, calibrating Stark plates, and due to its pungent aroma, it is also easy to notice leaks.

For one reason or another, our bottle of OCS was mixed with xenon as the carrier gas. The fact that we could observe the Xe···OCS complex is not particularly surprising, as many OCS complexes have been studied previously, including complexes of OCS with a single atom[3–9] or a di-/tri-atomic partner.[10–12] Initially, we thought that somebody must have studied this complex before, as it is the last one in series of OCS complexes

with non-radioactive noble gases. However, it does not seem to be the case, and it is up to us to fill this particular gap in this series of homologues.

However, despite the somewhat serendipitous impetus behind this opus, the Xe···OCS complex is far from a gap-filler. There are 6 stable and relatively abundant ($>4\%$) isotopes of Xe, in addition to the abundant ^{13}C and ^{34}S isotopologues of OCS. As only 6 structural parameters are necessary to fully define the geometry of any tetratomic species (4 parameters, if we assume OCS is linear and the complex is planar), it is possible to obtain a purely experimental near-equilibrium structure of Xe···OCS. We have previously investigated three of the rare gas (Rg) complexes of OCS, providing semi-experimental equilibrium structures (r_e^{SE}) of the Ne, Ar, and Kr isomorphs.[13] In the current work we (i) determine analogous r_e^{SE} structures of the He, and Xe complexes, completing the Rg···OCS series, and also include the Hg···OCS complex for comparison. Then we (ii) report the fully-experimental $r_m^{(2)}$ structure of the Xe···OCS complex. Finally, we (iii) push the limits of correlated wavefunction theory (WFT) to explain the differences between the observed $r_m^{(2)}$ structure and the calculated r_e and semi-experimental r_e^{SE} structures of the Xe···OCS complex. As foreshadowed in the title of the current work, particular attention will be paid to relativistic effects, and the deformation of the O=C=S monomer upon complexation.

2 Experimental methods

After initial discovery of possible Xe···OCS transitions, broadband spectra were collected on the In-phase/quadrature-phase Modulation Passage-Acquired-Coherence Technique (IMPACT) spectrometer.[14] The presence of the xenon complex was quickly confirmed thanks to the distinctive pattern of the six main

[a] *Theoretical Chemistry, Leibniz Universität Hannover, Callinstrasse 3A, 30167 Hannover, Germany. E-mail: peter.kraus@theochem.uni-hannover.de*

[b] *Institut für Physikalische Chemie und Elektrochemie, Leibniz Universität Hannover, Callinstrasse 3A, 30167 Hannover, Germany*

† All computational inputs and outputs, SPFIT and STRFIT files, an overview of isotopologue data, measured transitions, XYZ structures, as well as scripts required to reproduce the figures are attached. See DOI: 10.5281/zenodo.3582270.
‡ Electronic supplementary information (ESI) available. See DOI: 10.1039/d0cp00334d
§ These authors contributed equally to this work.
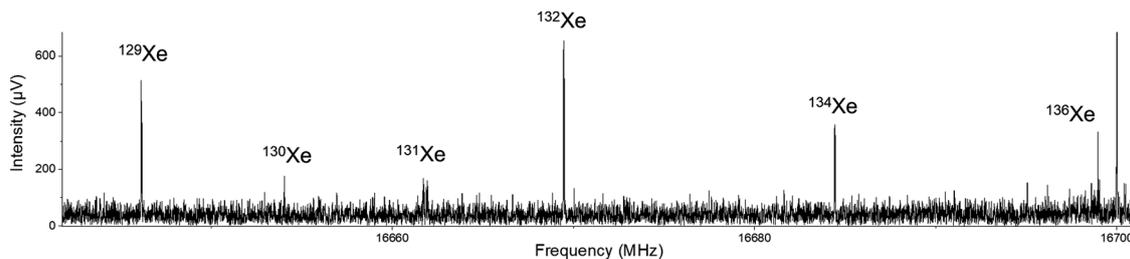¶ COBRA stands for Coaxially Oriented Beam-Resonator Arrangement.

This journal is © the Owner Societies 2020

Phys. Chem. Chem. Phys., 2020, **22**, 5615–5624 | 5615

Fig. 1 The $6_{24} \leftarrow 6_{15}$ transitions for the six most abundant xenon isotopes. The intensity pattern follows the relative abundances of each isotope, with the exception of ^{131}Xe, which is split into nuclear hyperfine components ($I_{^{131}Xe} = 3/2$). The spike at 16 700 MHz is a carrier frequency signal.

xenon isotopologues: ^{132}Xe (26.9%), ^{129}Xe (26.4%), ^{131}Xe (21.2%), ^{134}Xe (10.4%), ^{136}Xe (8.9%), and ^{130}Xe (4.1%). An example transition is shown in Fig. 1. This spectrum can also serve as a pedagogical example of how isotopic shifts of transitions can be related to changes in mass in a nearly-rigid rotor.

Up to this point, all measurements were made using 1% OCS (Air Products) in pure Xe. To save on the expensive xenon, further measurements were made with a mixture of 1% OCS and 1% xenon in argon. Signals were slightly better in argon expansions than in pure xenon. Backing pressures of 0.7–1.5 bar absolute pressure were used for both carrier gases. With the broadband spectra and assignments as a guide, the sample was brought back to the Coaxially Oriented Beam-Resonator Arrangement (COBRA) spectrometer to complete the measurement of the nine reported isotopologues. The strongest transitions were observed for the μ_b selection rule, the μ_a dipole transitions were observed only for the most abundant isotopologues. Fit results of the parent isotopologue are shown in Table 1 where they are compared to selected computational methods. Fits for all isotopologues, including centrifugal distortion constants and inertial defects for the parent species, are included in the ESI.‡

3 Computational details

All density functional theory (DFT) calculations are performed using Gaussian,[15] using the G09.E01 and G16.A03 revisions. The three density functional approximations (DFAs) used in the current work are chosen to explore the trends in anharmonic vibration–rotation interaction constants (α_i) when climbing the "Jacob's ladder" of DFT: they are the generalized gradient approximation BLYP,[16,17] the global single hybrid B3LYP,[18,19]

and the double hybrid B2PLYP.[20] All three functionals are always applied with the D3(BJ) empirical dispersion correction,[21,22] counterpoise correction,[23] and the Dunning-type 3-ζ basis set augmented by diffuse functions,[24] with the appropriate effective core potentials (PP) for Xe[25] and Hg.[26] For the B2PLYP functional, frozen-core approximation is always applied. In the following text, BLYP, B3LYP, and B2PLYP are used instead of the CP-[B,B3,B2P]LYP-D3(BJ)/aug-cc-pVTZ-[PP] notation. Tighter geometry convergence criteria for forces (max. <2 μE_h a$_0^{-1}$, RMS <1 μE_h a$_0^{-1}$) and displacements (max. <6 μa$_0$, RMS <4 μa$_0$) and a "superfine" (250, 974) grid are applied in all DFT calculations.

The anharmonic vibration–rotation interaction constants determined at the coupled cluster level of theory[27] for the He, Ne and Ar complexes are calculated using Cfour.[28] The basis sets used here are identical to the 3-ζ augmented basis sets used with in the DFT calculations. Frozen-core approximation is always applied. The geometries are optimized with a threshold for RMS of the gradient <10 μEh a$_0^{-1}$. In the following text, CCSD(T) is used instead of the FC-CCSD(T)/aug-cc-pVTZ notation.

The symmetry adapted perturbation theory (SAPT) calculations are performed in Psi4[29] version 1.3. The SAPT2+(CCD)δMP2 variant is applied with the 3-ζ augmented basis sets, following the recommendation of Parker et al.[30] The 5-ζ variants are used as density fitting bases. The r_e^{SE} structures based on B2PLYP corrections are used in this set of calculations. In the following text this method is simply called SAPT.

The extrapolated WFT calculations are performed in Psi4[29] version 1.3rc1 and later. The extrapolation recipe consists of a Hartree–Fock component (HF/cc-pwcV[TQ5]Z), a MP2 component (MP2/cc-pwcV[Q5]Z), and a CCSD(T) correction to the MP2 correlation (ΔCCSD(T)/cc-pwcV[TQ]Z). All correlated levels of wavefunction theory are used with the frozen-core approximation, with density fitting used throughout. The weighted core-valence basis sets[31] of 3-, 4-, and 5-ζ quality are used here, with the appropriate effective core potentials (ECP) for Kr, Xe, and Hg atoms. The default auxiliary basis sets for density fitting (up to def2-QZVPPD) are used throughout this work. The extrapolation is performed using the "cubic" Helgaker extrapolation formulas.[32] This extrapolation method is called MP2+δ(T) in the following text.

Further corrections are applied to the MP2+δ(T) level of theory in the study of the Xe···OCS complex: the all-electron correlation, denoted δ_{FC}^{AE}, is estimated by the difference of

Table 1 Vibrational ground state average rotational constants (B_0) including centrifugal distortion terms calculated using BLYP, B3LYP, and B2PLYP are compared to the experimental results for the ^{132}Xe$\cdots^{16}$O^{12}C^{32}S species. The DFAs are applied with a counterpoise correction, D3(BJ) dispersion correction, and an augmented 3-ζ basis set

	BLYP	B3LYP	B2PLYP	^{132}Xe
A_0 (MHz)	6308.90	6450.10	6484.08	6555.58843(43)
B_0 (MHz)	774.967	783.848	778.667	770.764639(77)
C_0 (MHz)	688.036	686.789	692.998	687.367332(40)
N	—	—	—	131
RMS (kHz)	—	—	—	1.6

5616 | *Phys. Chem. Chem. Phys.*, 2020, **22**, 5615–5624

This journal is © the Owner Societies 2020

CCSD(T)/TZP calculations with and without frozen core approximation. To gauge relativistic effects, calculations at the CCSD(T)/TZP-DKH level with the 2nd or 4th order Douglas–Kroll–Hess Hamiltonian are compared to the CCSD(T)/TZP calculations. This correction is denoted $\delta_{rel}^{[2,4]}$, and it is computed using the DKH interface[33] in Psi4, with conventional CCSD(T) used instead of the density-fitted variant in the MP2+δ(T) recipe. The TZP-DKH and TZP basis sets are the 3-ζ quality basis sets from Campos and Jorge[34] designed for use with and without the Douglas–Kroll–Hess Hamiltonian. Finally, to estimate the effects of diffuse functions on the structure, the aug-cc-pwCV[TQ5]Z basis sets for O, C and S are paired with the cc-pwCV[TQ5]Z-PP basis set for Xe, augmented by diffuse functions from the aug-cc-pV[TQ5]Z-PP basis sets. The results of this calculation are denoted as aug-MP2+δ(T).

All r_0, r_e^{SE}, and $r_m^{[[1,2]]}$ structures are fit directly to the rotational constants using STRFIT[35] version 8a.X.2016.[36] All Gaussian, Cfour, and Psi4 input/output files are included in the ESI.‡

4 Results and discussion

4.1 Semi-experimental structures with DFT corrections

The experimental rotational constants at the vibrational zero-point level (B_0) can be used to determine a vibrationally averaged ground state structure (r_0). Assuming the OCS monomer remains rigid upon complexation with a rare gas atom, the C$\cdots$Rg distance and O–C$\cdots$Rg angle are enough to determine the structure by fitting the measured rotational constants. The same process can be applied to rotational constants, that are corrected towards their equilibrium counterparts (B_e). A semi-experimental correction uses the anharmonic vibration–rotation interaction constants α_i to calculate the vibrational corrections ΔB_e^{DFT} from eqn (1).

$$\Delta B_e^{DFT} = \frac{1}{2}\sum_i \alpha_i \tag{1}$$

The summation runs over all i vibrational modes for each rotational constant. The α_i values are obtained from second order vibrational perturbation theory[37] applied to potential energy surfaces calculated using DFT. The semi-experimental equilibrium rotational constants can then be calculated according to eqn (2)

$$B_0 = B_e + \Delta B_e^{DFT} \tag{2}$$

In principle, both electronic and vibrational effects should be considered in the ΔB_e terms. However, the electronic contribution to the ΔB_e^{DFT} corrections is in the kHz range for the OCS complexes,[13] well within the uncertainty of the vibrational correction. Therefore, we have omitted it in this work. As in our previous investigation,[13] the r_0 and r_e^{SE} structures are fitted to the rotational constants along the a and c axes. The planar structure of the complexes means the rotational constants are correlated, and the inclusion of the third constant would lead to a decreased quality of the fit. It could be argued, that all experimentally available information should be
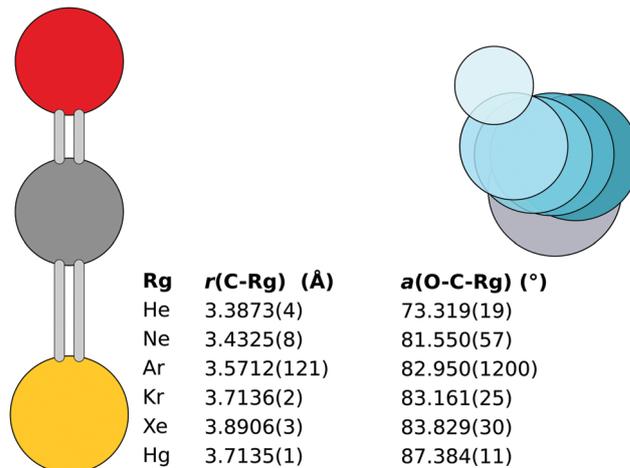

Fig. 2 The r_e^{SE} structures of the six OCS complexes obtained with B2PLYP corrections. Note: the $r(C–Ar)$ with the ^{18}O isotopologue excluded is 3.5598(3) Å.

Rg	r(C-Rg) (Å)	a(O-C-Rg) (°)
He	3.3873(4)	73.319(19)
Ne	3.4325(8)	81.550(57)
Ar	3.5712(121)	82.950(1200)
Kr	3.7136(2)	83.161(25)
Xe	3.8906(3)	83.829(30)
Hg	3.7135(1)	87.384(11)

used in the fit, and that any associated decrease in the quality of the fit reflects the errors in either the ΔB_e^{DFT} or the fit itself. We have considered this issue, and prefer to remain consistent with previous work. As mentioned above, the equilibrium structure of the OCS monomer is kept rigid and linear. The bond lengths of Morino and Matsumura[1] are used for all r_0 and r_e^{SE} structures.

Unlike in the previous work, the initial fit reported here takes into account all available isotopologue data.‖ The resulting r_e^{SE} structures obtained with B2PLYP corrections are shown in Fig. 2. The structures obtained using B3LYP and BLYP are listed in the ESI.‡

The monomer separation increases down the rare gas group. The O–C$\cdots$Rg angle increases with increased molecular weight of the Rg atom. An exception is the Hg$\cdots$OCS complex, which has a monomer separation comparable to the Kr complex, despite the Hg atom being significantly heavier than Kr and even Xe. This shorter distance hints at a different bonding mechanism in the complex.

For the heavier complexes, the r_e^{SE} structures obtained with B2PLYP, B3LYP, and BLYP are comparable. This lends confidence to the quality of the structures. In Hg$\cdots$OCS the B2PLYP structure differs from B3LYP and BLYP by less than 3 mÅ, attributed to the different ΔB_e^{DFT} along the c axis (1.2 vs. 2.1 and 2.2 MHz, respectively). For Xe$\cdots$OCS the three structures agree within 1 mÅ. The largest relative deviation in the obtained rotational constants is observed for the A rotational constant, as shown in Table 1. In the case of Kr$\cdots$OCS the B3LYP structure differs by 7 mÅ from the other two due to an outlier in ΔB_e^{DFT} along the A axis for the parent isotopologue.

‖ For He$\cdots$OCS: the parent, ^{13}C, and ^{34}S isotopologues;[9] for Ne$\cdots$OCS: the parent, ^{21}Ne, ^{22}Ne, ^{18}O, ^{13}C, ^{33}S, and ^{34}S isotopologues;[6] for Ar$\cdots$OCS: the parent, ^{17}O, ^{18}O, ^{13}C, and ^{34}S isotopologues;[5] for Kr$\cdots$OCS: the ^{82}Kr, ^{84}Kr, and ^{86}Kr isotopologues;[3] for Hg$\cdots$OCS: the ^{198}Hg, ^{199}Hg, ^{200}Hg, ^{201}Hg, ^{202}Hg, and ^{204}Hg isotopologues;[4] for Xe$\cdots$OCS: the ^{129}Xe, ^{129}Xe^{34}S, ^{130}Xe, ^{131}Xe, ^{132}Xe, ^{132}Xe^{13}C, ^{132}Xe^{34}S, ^{134}Xe, and ^{136}Xe isotopologues.

This journal is © the Owner Societies 2020

Phys. Chem. Chem. Phys., 2020, **22**, 5615–5624 | **5617**

In Ar···OCS, the B2PLYP-based ΔB_e^{DFT} results are affected by an inconsistency in the [18]O isotopologue, for which the corrections to B_0 and C_0 are opposite in sign compared to the parent isotopologue (see ESI‡).[13] Hence the somewhat large error in the bond length shown in Fig. 2. A CCSD(T) calculation of the parent isotopologue produces vibration–rotation interaction constants in line with the B3LYP and B2PLYP results. With the [18]O isotopologue excluded from the B2PLYP-based fit, the B3LYP and B2PLYP structures agree to 1 mÅ with $r(C\cdots Ar) = 3.5598(3)$ for the B2PLYP variant.[13] This structure is used as the r_e^{SE} in the following text. The BLYP functional predicts a 43 mÅ longer separation.

In the lightest two complexes, some of the DFAs yield negative frequencies when anharmonic corrections are applied to the (positive) harmonic frequencies. Two negative frequencies can be observed in the BLYP results for Ne···OCS, one can be observed in both B2PLYP and B3LYP results for the He···OCS complex. The weakly bound intermonomer mode is always one of those problematic degrees of freedom. For the Ne···OCS complex the B2PLYP and B3LYP corrections are comparable and the r_e^{SE} structures differ by less than 3 mÅ. However, the CCSD(T) results for the parent isotopologue are inconsistent with the DFT calculations.

The story is similar in the He···OCS complex. The B2PLYP-based r_e^{SE} follows the trend in bond lengths of the rare gas group, but the obtained angle is significantly different. On the other hand, the anharmonic frequencies obtained with BLYP do not have negative artefacts, and the angle in the BLYP structure of the He complex is more consistent with the rest of the dataset. However, the intermonomer separation obtained with BLYP is 3.7514(3) Å, which is longer than Kr···OCS and therefore unrealistic. The CCSD(T) structure has an angle similar to the BLYP structure, but the intermonomer separation of 3.233 Å is too short, even shorter than the B2PLYP result. Furthermore, the vibration–rotation interaction constants for the parent isotopologue are completely different between the CCSD(T) and the three DFAs. Therefore, the presented r_e^{SE} structures for the He and Ne complexes are unreliable.

4.2 Binding and interaction energies

The overall binding energy of a complex (D_E) can be defined as the experimentally observable change in the energy upon binding of the monomers. Ignoring basis set and size consistency errors, it can be thought of as the difference of the zero-point corrected energy of the complex from the sum of the zero-point corrected energies of the relaxed monomers. Alternatively, it can be thought of as a sum of the interaction energy (E_{int}), the deformation energy (ΔE_D) and the change in the zero-point energy (ΔE_{ZPE}). The interaction energy is widely used as a benchmark quantity for computational methods, as calculating E_{int} requires no geometry optimisation, but just a handful of single-point energy calculations.

As a first look on the trends in the interaction energies in this set, we have applied the SAPT decomposition to the B2PLYP-based r_e^{SE} geometries. The contribution of the SAPT components of the interaction energy is shown in Fig. 3.
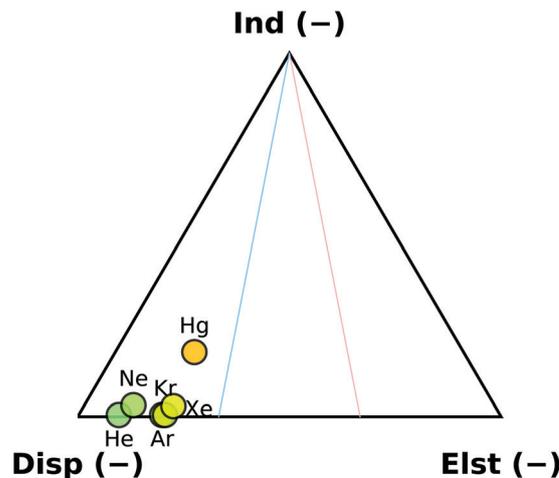

Fig. 3 SAPT decomposition of the interaction energies of the six studied OCS complexes. Energies obtained at the r_e^{SE} structures.

The interaction with the rare gases is completely dispersion dominated, with electrostatic contribution increasing slightly down the group. The trend can be attributed to an increasing polarisability of the atoms (1.38, 2.66, 11.08, 16.78, 27.32, and 33.91 a.u. for He, Ne, Ar, Kr, Xe, and Hg, respectively[38]). The sole exception is the non-rare gas Hg···OCS complex, where the interaction contains a significant induction contribution. The second-order $E_{ind,r}^{(20)}(A \leftarrow B)$ induction terms are responsible for this behaviour. In the rare gas complexes, the $E_{ind,r}^{(20)}(Rg \leftarrow OCS)$ and the $E_{ind,r}^{(20)}(OCS \leftarrow Rg)$ terms are approximately equal, while in Hg···OCS, the $E_{ind,r}^{(20)}(Hg \leftarrow OCS)$ term is ~10× higher than $E_{ind,r}^{(20)}(OCS \leftarrow Hg)$. At infinite separation, these contributions would be determined by the polarisation of A in the unperturbed static multipole of B.[39] As shown above, the difference in the static polarisability of Xe and Hg is smaller than between Kr and Xe, therefore this behaviour must have a different cause: at finite separations, the polarisation propagators of the monomers become important.[39] It has been previously shown, that a simple electrostatic model is able to reproduce the induced dipole in the Rg···CO₂ series, while it fails for Hg···CO₂.[40] In the OCS complexes, the predicted dipole moment along the Rg···C direction decreases along the group from 0.33 Debye for He down to a minimum of ~0.17 Debye in the Kr and Xe complexes. In Hg···OCS the calculated dipole moment is higher again at 0.28 Debye. We attribute this behaviour to the empty p-orbitals on Hg, which enable additional flexibility in the polarisation of the system compared to the noble gas complexes.

The SAPT interaction energies are compared to the counterpoise-corrected MP2+δ(T) interaction energies at the optimized geometries in Table 2. Literature counterpoise-corrected CCSD(T)/aug-cc-pVTZ values of E_{int} for the Ne[8] and Ar[41] complexes, along with a CCSD(T)/aug-cc-pVQZ value for the He[42] and Kr complexes[43] are also shown in Table 2. For the lighter two complexes, the literature values are in a great agreement with our SAPT results. This is not surprising as the geometries used by Feng et al.[43] are not too different from our r_e^{SE}'s. However, our MP2+δ(T) results differ significantly

Table 2 Interaction (E_{int}) and binding (D_E) energies of the OCS complexes, in kJ mol^{-1}, calculated using SAPT, MP2+δ(T), from literature.[8,41–43] An experimental estimate obtained with a Lennard-Jones fit and the diatomic approximation is included for comparison. For a further set of D_E values, see the ESI

Complex	SAPT E_{int} @ r_e^{SE}	Lit. CCSD(T) E_{int}	MP2+δ(T) E_{int} @ r_e	D_E @ r_e	Experiment D_E @ r_0
He$\cdots$OCS	−0.510	−0.519	−0.478	−0.035	−0.152
Ne$\cdots$OCS	−0.964	−0.975	−0.709	−0.381	−0.518
Ar$\cdots$OCS	−2.491	−2.653	−2.434	−2.007	−1.943
Kr$\cdots$OCS	−3.079	−3.249	−3.314	−2.871	−2.536
Xe$\cdots$OCS	−3.665	—	−4.025	−3.827	−3.158
Hg$\cdots$OCS	−5.015	—	−4.570	−4.148	−3.157

from the other results. For the Ne$\cdots$OCS complex the significantly different geometry ($\sim$0.1 Å) is a likely cause. For the other complexes, the use of the 3-ζ basis sets in the literature and SAPT data introduces a basis set incompleteness error. The MP2+δ(T) values reported here should be of significantly higher accuracy: the energies are calculated at the respective fully-relaxed minima, and the correlation is obtained from larger basis sets, as well as extrapolated towards the complete basis set limit.

A set of experimental estimates of the binding energy is obtained from experimental rotational constants (B, C) and is also shown in Table 2. A diatomic approximation is used to estimate the force constant between the two monomers (k_s) from the centrifugal distortion constant (eqn (3)). Then this force constant is used to fit a Lennard-Jones model (eqn (4)).[44]

$$k_s = \frac{16\pi^2 \mu^2 R_{cm}^2 \left(3B^4 + 3C^4 + 2B^2C^2\right)}{hD_J} \quad (3)$$

$$D_E = -\frac{1}{72} k_s R_{cm}^2 \quad (4)$$

Here R_{cm}^2 is the center-of-mass separation of the monomers obtained from the experimental ground-state geometries (r_0), μ is the reduced mass of the complex, h is the Planck constant, and D_J is the centrifugal distortion constant. While the R_{cm}^2 should be derived from the equilibrium geometries,[44] we have opted to base this analysis on experimentally observed results. The substitution of r_0 and B_0-based values for r_e^{SE} and B_e^{SE}-derived ones, respectively, causes only a negligible difference in the binding energies of at most 40 J mol^{-1}. For a comparison of D_E values based on r_0, r_e^{SE}, and r_e^{DFT}, see Table S12 in the ESI.‡ The rotational and centrifugal constants are taken from the original publications.[3–6,9] Where necessary, the constants are refit with Watson's S-reduced Hamiltonian[45] using Kisiel's Convc utility (version 11.XIIa.1998).[36]

Such experimental binding energies are generally valid under two assumptions: (i) the center-of-mass axis of the monomers is approximately parallel with the a axis of inertia, and (ii) the centrifugal distortion is mainly due to a single vibrational mode along the center-of-mass axis. While the latter is true for all of the studied complexes, the former approximation is only valid from Ar$\cdots$OCS down the group.

The agreement between the experimental estimates and the calculated D_E data is remarkably good for the rare gas complexes (within "chemical accuracy" of 0.4 kJ mol^{-1}), given how naïve such a fit to a Lennard-Jones model is. The Hg$\cdots$OCS complex is again an outlier: the experimental binding energy is significantly weaker than the calculated value. Relativistic effects are likely to play a significant role in both Hg and Xe complexes. Such effects are "included" implicitly in the experimental value, but in MP2+δ(T) they are treated only in the ECP of the basis set. See further remarks on relativistic effects below. For Hg$\cdots$OCS, a rough estimate of the relativistic effects in the interaction energy can be obtained at the MP2+δ(T) level by replacing the 60-electron relativistic ECP by a 60-electron non-relativistic one. The non-relativistic E_{int} of −2.918 kJ mol^{-1} is 1.562 kJ mol^{-1} lower than the result with the relativistic ECP. The better agreement with the experimental value is likely purely coincidental. For Xe$\cdots$OCS, we had to resort to an estimate using CCSD(T) with all-electron [TQ]ZP and [TQ]ZP-DKH basis sets[34] used with and without second order Douglas–Kroll–Hess Hamiltonian, respectively. The non-relativistic E_{int} is 1.306 kJ mol^{-1} lower than the relativistic one, similar in magnitude and direction to the Hg$\cdots$OCS case.

The Lennard-Jones model can be in principle cross-checked for validity using calculated data. This is achieved by using the R_{cm}'s from the r_e^{B2PLYP} structures, along with the associated rotational constants, as well as the centrifugal distortion constant D_J^{B2PLYP} obtained using second-order vibrational perturbation calculations. The results are shown in Table S12 in the ESI.‡ The binding energies obtained using the supermolecular approach (i.e. from $E_{complex} - \sum E_{monomers}$) should be identical to the Lennard-Jones model when B2PLYP-derived data is used in both. The large discrepancy between the r_e^{B2PLYP} results and all other results is due to the significant underprediction of the centrifugal distortion constants: for instance, in the He$\cdots$OCS complex, B2PLYP and second-order vibrational perturbation theory predict a D_J^{B2PLYP} of 79.05 kHz, while the experimental value is 438.63 kHz.

Predicting accurate centrifugal distortion constants is a difficult task. In diatomics, the predicted D_J's from wavefunction theory (CCSD(T)/aug-cc-pVTZ) and density functional theory (B3LYP/aug-cc-pVTZ) are comparable, within 10% of experimental values.[46] The agreement worsens significantly for the polyatomic CH_2PCl: CCSD(T)/cc-pVQZ results are within 25% of the experiment, while upon application of second-order vibrational perturbation theory, or single-hybrid DFAs, the deviation from experiment increases.[47] Therefore, the disagreement between the binding energies from the supermolecular and Lennard-Jones approach reflects the innacurate D_J^{B2PLYP} as opposed to an invalidity of the Lennard-Jones model.

The deformation energies for all complexes are negligible when compared to the overall binding energies. In the rare gas complexes, the OCS deformation energies are in the 1–3 J mol^{-1} range. For these complexes, the O–C–S angle bends towards the rare gas atom by at most 0.2°. In the Hg$\cdots$OCS the deformation energy is slightly higher at 18 J mol^{-1}, and the O–C–S bend reaches 0.3°. While it would seem that the deformation of the

This journal is © the Owner Societies 2020

Phys. Chem. Chem. Phys., 2020, **22**, 5615–5624 | **5619**

OCS monomer increases with increasing binding energy, this is not true for OCS complexes in general. The $CS_2 \cdots OCS$ complex has an interaction energy of ~ 8 kJ mol^{-1}, but the OCS molecule is deformed by less than $0.1°$ at a similar level of theory.[48] The zero point energy differences show no particular trends, with the lowest difference calculated for $Xe \cdots OCS$ (0.196 kJ mol^{-1}) and the highest for $He \cdots OCS$ (0.442 kJ mol^{-1}).

4.3 Interaction energy surfaces

An interaction energy surface of the $He \cdots OCS$ dimer calculated with SAPT is shown in Fig. 4. The energy surfaces of the other dimers differ only quantitatively. The two adjusted parameters are the $C \cdots Rg$ distance and $S-C \cdots Rg$ angle. The OCS monomer was held at the equilibrium bond length.[1]

The potential surface of the He complex contains the global minimum, as well as two local minima: the linear conformations $He \cdots SCO$ and $SCO \cdots He$. The sulphur-bound conformer is more strongly bound of the two, with an interaction energy of $\sim 70\%$ of the global minimum. The oxygen-bound conformer is more weakly bound, and for heavier complexes (Kr onwards) this stationary point becomes a transition state. The SAPT surfaces show the same features as the potential surfaces of He,[42] Ne,[8] Ar,[41] and $Kr \cdots OCS$[43] complexes. The shape of the potential surface near the global minimum is extremely flat and asymmetric. In fact, for the $He \cdots OCS$ species with a calculated D_E of -35 J mol^{-1} (at 0 K, see Table 2), it is surprising an experimental observation of the complex was possible at all.

4.4 Mass-dependent structures of $Xe \cdots OCS$ and $Ne \cdots OCS$

An appealing alternative to the semi-experimental method for obtaining near-equilibrium structures is the mass-dependent approach of Watson.[49] As above, the equilibrium moments of inertia (I_e) can be obtained from the experimental moments of inertia at the vibrational ground state (I_0) and a vibrational zero-point correction (ε_0). In a departure from the semi-experimental treatment, in the mass-dependent structures the

vibrational corrections are fitted to experimental data according to eqn (5).

$$\varepsilon_0 = c(I_e)^{1/2} + d \left(\frac{\prod_i^N m_i}{M} \right)^{1/(2N-2)} \tag{5}$$

Here m_i is the mass of atom i, N is the total number of atoms in the species, and M is the total mass of the species. The parameters c and d are two sets of fitted constants. The c correction terms account for the isotope dependence of ε_0, while the d correction terms are designed to remedy issues with small atomic coordinates.[50] Structures where only c_α values are determined (α = A, B, C) are denoted $r_m^{(1)}$. When both c_α and d_α are fitted, the structures are denoted $r_m^{(2)}$. For covalently bound linear triatomics, the $r_m^{(2)}$ structures can be expected to be accurate to ~ 1 mÅ of the true r_e structure.[50] While the differences are likely to be larger for van der Waals complexes, the mass-dependent structures are "probably the best currently available tool for determining meaningful geometries for weakly bound clusters on the basis of only the ground state rotational constants."[35]

With a measurement of 9 isotopologues of $Xe \cdots OCS$, it is possible to fit the 5 structural parameters required to fully define the structure of the planar complex, as well as the c and d coefficients. The fitted parameters are the $C \cdots Xe$, $C=O$, and $C=S$ lengths, and the $O-C \cdots Xe$, and $O-C-S$ angles. Additionally, the full set of c_α's as well as d_A and d_B are fitted. The dihedral angle, as well as d_C, are not fit to ensure planarity. In total, 10 parameters are fitted to the 27 rotational constants to obtain the $r_m^{(2)}$ structure of $Xe \cdots OCS$. The $r_m^{(1)}$ structure was obtained analogously.

The only significant difference between the two mass-dependent structures is in the $O=C$ bond length. In the $r_m^{(2)}$ structure the bond is 20 mÅ longer than the equilibrium distance of OCS. In the $r_m^{(1)}$ the difference is only 10 mÅ. When the $O=C$ bond is held fixed to the shorter equilibrium bond length in OCS, the remaining structural parameters ($O=C=S$ angle, $C=S$ bond length and the Xe-dependent parameters) remain within the uncertainty of the fits and the degree of fit decreases slightly. Both r_m structures also show a bend in the OCS monomer of $\sim 1°$. From this data alone it is impossible to judge whether the distortion of the OCS monomer is an artefact of the fit.

The most striking difference between the $r_m^{(2)}$ and r_e^{SE} structures is in the 30 mÅ shorter $C \cdots Xe$ distance in the mass-dependent structure (see Fig. 5, as well as Fig. 2 for the r_e^{SE} structural parameters). The $1.3°$ higher $O-C \cdots Xe$ angle is mainly due to the $1.1°$ bend of the $O=C=S$ unit from a linear shape. The intermonomer potential in the $r_m^{(2)}$ structures is shifted slightly towards the S atom.

A comparison with the equilibrium structure obtained using MP2+δ(T) reveals that the chosen level of wavefunction theory predicts a significantly shorter monomer separation compared to the mass dependent as well as the semi-experimental structures (by 43 mÅ and 73 mÅ, respectively). The $O=C \cdots Xe$ angle from MP2+δ(T) is almost identical with the r_e^{SE} structure.
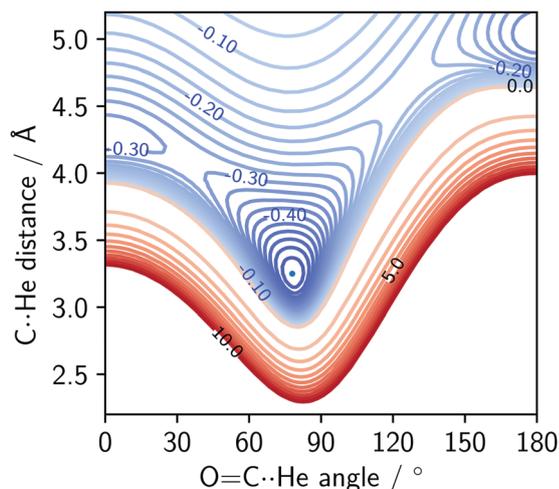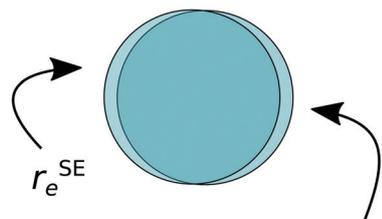

Fig. 4 SAPT interaction energy surface of the $He \cdots OCS$ complex. Energies in kJ mol^{-1}. Blue contours represent binding (spacing 0.025 kJ mol^{-1}), red represent repulsion (spacing 1 kJ mol^{-1}).

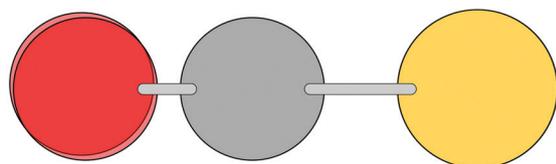|		$r_e^{MP2+\delta(T)}$	$r_m^{(2)}$	r_e^{SE}
r(C-Xe)	(Å)	3.8184	3.8602(3)	3.8906(3)
r(O=C)	(Å)	1.1578	1.1774(29)	1.1570
r(C=S)	(Å)	1.5641	1.5548(10)	1.5608
a(O-C-Xe)	(°)	83.914	85.156(27)	83.829(30)
a(O-C-S)	(°)	179.838	178.949(36)	180.0

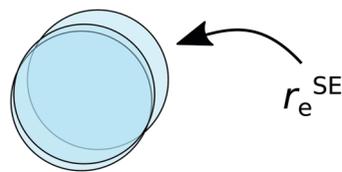**Fig. 5** The semi-experimental (r_e^{SE}), mass-dependent ($r_m^{(2)}$), and theoretical ($r_e^{MP2+\delta(T)}$) structure of Xe···OCS.

		$r_e^{MP2+\delta(T)}$	$r_m^{(2)}$	r_e^{SE}
r(C-Ne)	(Å)	3.3162	3.2754(168)	3.4325(8)
r(O=C)	(Å)	1.1575	1.0940(164)	1.1570
r(C=S)	(Å)	1.5642	1.5336(194)	1.5608
a(O-C-Ne)	(°)	79.638	82.520(1072)	81.550(57)
a(O-C-S)	(°)	179.976	182.466(1469)	180.0

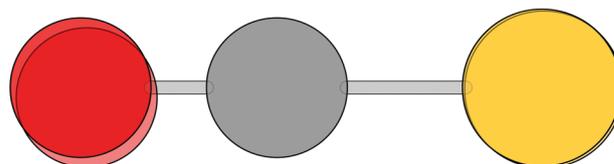**Fig. 6** The semi-experimental (r_e^{SE}), mass-dependent ($r_m^{(2)}$) and theoretical ($r_e^{MP2+\delta(T)}$) structure of Ne···OCS.

The OCS monomer in the r_e^{SE} structure is only slightly distorted from the equilibrium values, with a 0.2° inward bend. This leads us to two conclusions: (i) the OCS monomer remains at near-equilibrium values, and the significant deviations of the OCS moiety from its equilibrium shape in both r_m structures can be attributed to the fitting process, and (ii) an effect unaccounted for in the MP2+δ(T) method leads to a larger monomer separation in the experimental results.

As 7 isotopologues of the Ne···OCS complex have been measured by Xu and Gerry,[6] it is possible to apply the above fitting process to that set of rotational constants. The resulting $r_m^{(2)}$ structure is compared to the r_e^{SE} structure with B2PLYP-based corrections and the $r_e^{MP2+\delta(T)}$ structure in Fig. 6.

The issues with the r_e^{SE} structure are obvious at the first glance: the C···Ne distance is longer by ∼140 mÅ compared to the other two structures, and the angle is also significantly different. As a very similar r_e^{SE} structure has been obtained with B3LYP-based corrections, this inaccuracy is unlikely due to the DFA itself, but more likely a failure of the vibrational perturbation theory for such shallow modes. The frequency shift of the C···Ne stretch into the imaginary region upon anharmonic correction supports this argument.

There are significant differences in the $r_m^{(2)}$ and $r_e^{MP2+\delta(T)}$ structures. The position of the O-atom in the $r_m^{(2)}$ structure is troublesome, despite including the ^{18}O isotopologue in the fit. At 1.094 Å, the O=C bond is unphysically short, and the O–C–S angle is over 180°, meaning the OCS molecule deflects away from the Ne atom. Unfortunately, fixing individual OCS parameters leads to a much poorer fit. When the O=C distance is fixed to the equilibrium

value, the structure fit doesn't converge, unless both C=S length and O–C–S angle are also fixed. The best option seems to be to fix the O–C–S angle to 180°. This forces the O=C bond to shrink even further, but brings the C···Ne bond length within 14 mÅ of the MP2+δ(T) value. Finally, while the d-contributions in the $r_m^{(2)}$ fit are associated with a large uncertainty, simply removing them doesn't alleviate the issues with the structure. The $r_m^{(1)}$ and $r_m^{(2)}$ structures are essentially identical.

4.5 Chasing experimental accuracy with wavefunction theory

The MP2+δ(T) recipe contains a Hartree–Fock component calculated from a [3,4,5]-ζ extrapolation. The correlation energy is calculated from two components: a second-order Møller–Plesset component calculated in an extrapolated [4,5]-ζ basis, and a higher-order correlation correction obtained from a difference in CCSD(T) and MP2 energies in an extrapolated [3,4]-ζ basis.

The Hartree–Fock component is likely to be converged to the complete basis set limit.[51] The convergence of the correlation energy is not so certain, and can be improved in three ways: (i) by calculating correlation at a higher level of theory, (ii) by using a larger basis set or adding diffuse and/or midpoint functions, or (iii) by correlating all electrons in the calculation. Higher level correlation in dispersion-dominated complexes of similar interaction energies was studied by Řezáč and Hobza:[52] the CCSDT(Q) correction to a CCSD(T) energy accounts for only 1–3% of the interaction energy. Due to the enormous computational cost of CCSDT(Q) calculations, we currently cannot investigate higher order effects on this system.
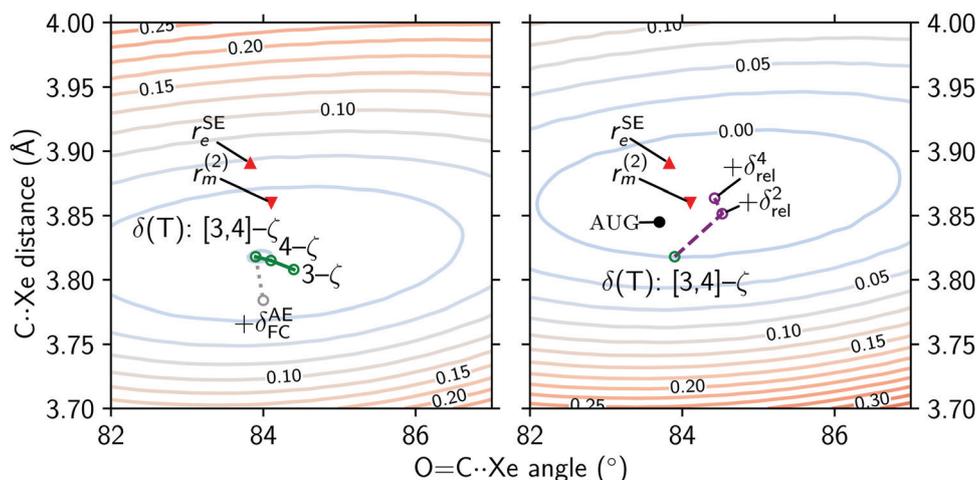
This journal is © the Owner Societies 2020

Phys. Chem. Chem. Phys., 2020, **22**, 5615–5624 | **5621**

Fig. 7 The potential energy surface of Xe⋯OCS. Left: The MP2+δ(T) surface overlaid with points showing the effect of increasing basis set size (green) and the all electron correction (gray) on the structure. Right: The MP2+δ(T) + δ_{rel}^4 surface overlaid with points showing increasing order in the DKH Hamiltonian (purple). The results of the calculation with additional diffuse functions in the basis sets (aug-MP2+δ(T)) are also shown (black). Points corresponding to the semi-experimental and mass-weighted structure (red) are included for comparison. Contours correspond to energies above the MP2+δ(T) minimum, in kJ mol^{-1}.

Basis set incompleteness at the CCSD(T)/[3,4]-ζ level is about ~ 50 mÅ in the very weakly bound Ar⋯Ar complex, and decreases to ~ 5 mÅ for a more strongly bound complex, such as NH$_3$⋯HF.[53] The effect of increasing basis set size in the δ(T) component of the MP2+δ(T) recipe is shown in Fig. 7, in the left panel. Note that the O=C⋯S angle in the $r_m^{(2)}$ structure (▼) is adjusted here by assuming the OCS monomer is linear. With increasing basis set size (○), the intermonomer distance hardly changes, and the main difference is in the O=C⋯Xe angle. This further confirms that the structure is likely near convergence with respect to basis set size.

We have investigated two additional basis set effects: counterpoise correction for the basis set superposition error, and the effect of diffuse functions. The former has no significant effect on the structure, as the difference in the monomer separation obtained from MP2+δ(T) and CP-MP2+δ(T) is only 0.001 Å. On the other hand, the aug-MP2+δ(T) structure obtained with cc-pwCV[TQ5]Z basis sets augmented by diffuse functions (see in Fig. 7) is remarkably close to the experimental $r_m^{(2)}$ structure, with a disagreement in the monomer separation of only 15 mÅ. While this is most certainly a step in the right direction, the increased computational cost compared to cc-pwCV[TQ5]Z calculations is immense: the augmentation of the basis set increases the number of basis functions by 20%, and the amount of memory required for the computation of the connected triples (i.e. the (T) component) more than doubles. Notably, additive terms obtained from the differences of augmented and unaugmented 3-ζ calculations that are used in various extrapolation recipes do not perform well for non-covalent complexes.[53,54] Therefore CCSD(T) computations with augmented 4-ζ basis sets might be unavoidable. Unfortunately, the currently available set of "aug-cc-pwCVnZ"-quality basis sets is limited to the first two periods in the main group and first row transition metals, and appropriate density fitting basis sets are also unavailable.

When the effect of correlating all core electrons is added to the MP2+δ(T) potential surface (○), the minimum in the potential moves even further away from the $r_m^{(2)}$ and r_e^{SE} results. This could be an incompatibility of the cc-pwcV[TQ]Z-PP basis sets used for the frozen-core components with the all-electron TZP basis set used to calculate the δ_{FC}^{AE} (as AE-CCSD(T)/TZP − FC-CCSD(T)/TZP). An all-electron 4-ζ CCSD(T) geometry optimisation is currently prohibitively expensive.

On the right panel of Fig. 7 we illustrate the effect relativistic corrections have on the potential energy surface, as well as on the minimum structures. By adding 4-th order corrections using the Douglas–Kroll–Hess Hamiltonian to the MP2+δ(T) potential, we obtain a global minimum that is within 10 mÅ of the $r_m^{(2)}$ structure. The O=C⋯Xe angle is also essentially the same when a linear OCS is assumed in the $r_m^{(2)}$ structure. However, it is worth noting that the relativistic effects are double counted in the right panel of Fig. 7: both scalar as well as spin–orbit effects are incorporated into the Xe effective core potentials,[25] the addition of the Douglas–Kroll–Hess correction treats the scalar relativistic effects a second time. These results confirm relativistic effects play an important role in the stabilisation of the Xe⋯OCS complex, but the agreement of the MP2+δ(T) + δ_{rel}^4 results with the $r_m^{(2)}$ structure is a case of obtaining a correct answer for the wrong reasons.

5 Conclusion

We present a (i) systematic computational study of OCS complexes with the noble gas group, (ii) an accurate structure of the Xe⋯OCS complex based on rotational spectroscopic data, and (iii) a detailed investigation into the geometry of the OCS monomer upon complexation.

The semi-experimental structures for the He and Ne complexes based on corrections obtained with DFT are unreliable.

This is attributed to a suspected breakdown of the second order vibrational perturbation theory for such flat intermolecular potentials. For the complexes of heavier atoms (Ar, Kr, Xe, Hg), the presented r_e^{SE} structures are significantly more reliable.

The binding mechanism in the rare gas complexes is dispersion dominated. In the Hg complex a small proportion of induction contributes to the binding, due to the empty p-shell of Hg. The calculated MP2+δ(T) binding energies D_E are in a good agreement with the experimental values using the Lennard-Jones model for complexes up to Kr. This agreement breaks down with in heavier complexes likely due to relativistic effects. The minor disagreement in the interaction energies compared to previous CCSD(T) literature data can be explained by basis set incompleteness in the literature results. The deformation of the OCS monomer from its equilibrium structure upon complexation is predicted to be minimal, with the largest bend of 0.3° predicted for Hg···OCS.

The mass-dependent $r_m^{(2)}$ structures of the Xe and Ne complexes differ significantly from the r_e^{SE} structures. The bond lengths and angles in the OCS monomer are distorted in the $r_m^{[[1,2]]}$ fits, especially the position of the O-atom. However, with the OCS monomer constrained to its equilibrium geometry, the mass-dependent structures are likely the most accurate structures ever obtained for the two complexes. The 43 mÅ difference in the monomer separation in the MP2+δ(T) and $r_m^{(2)}$ structures can be partially explained by the lack of diffuse functions in the cc-pwcVnZ basis sets: upon augmentation the difference drops to 15 mÅ. The closest agreement with the $r_m^{(2)}$ structure could be obtained by adding the 4-th order relativistic correction ($+\delta_{rel}^4$) to the MP2+δ(T) results, highlighting the importance of relativistic effects. However, this procedure cannot be generally recommended, as the scalar relativistic effects are double-counted. The inclusion of diffuse functions into at least 4-ζ basis sets is a more systematic way of converging towards experimental structures.

Conflicts of interest

There are no conflicts to declare.

Acknowledgements

Notes and references

1 Y. Morino and C. Matsumura, *Bull. Chem. Soc. Jpn.*, 1967, **40**, 1095–1100.

2 H. A. Dijkerman and G. Ruitenberg, *Chem. Phys. Lett.*, 1969, **3**, 172–174.

3 F. J. Lovas and R. D. Suenram, *J. Chem. Phys.*, 1987, **87**, 2010–2020.

4 M. Iida, Y. Ohshima and Y. Endo, *J. Chem. Phys.*, 1991, **94**, 6989–6994.

5 Y. Xu, W. Jäger and M. C. L. Gerry, *J. Mol. Spectrosc.*, 1992, **151**, 206–216.

6 Y. Xu and M. C. L. Gerry, *J. Mol. Spectrosc.*, 1995, **169**, 542–554.

7 J. Tang and A. R. W. McKellar, *J. Chem. Phys.*, 2001, **115**, 3053–3056.

8 H. Zhu, Y. Zhou and D. Xie, *J. Chem. Phys.*, 2005, **122**, 2–8.

9 Y. Xu and W. Jäger, *J. Mol. Spectrosc.*, 2008, **251**, 326–329.

10 J. J. Newby, M. M. Serafin, R. A. Peebles and S. A. Peebles, *Phys. Chem. Chem. Phys.*, 2005, **7**, 487–492.

11 Z. Yu, K. J. Higgins, W. Klemperer, M. C. McCarthy, P. Thaddeus, K. Liao and W. Jäger, *J. Chem. Phys.*, 2007, **127**, 054305.

12 M. Dehghany, J. N. Oliaee, M. Afshari, N. Moazzen-Ahmadi and A. R. W. McKellar, *J. Chem. Phys.*, 2009, **130**, 224310.

13 P. Kraus, D. A. Obenchain and I. Frank, *J. Phys. Chem. A*, 2018, **122**, 1077–1087.

14 M. K. Jahn, D. A. Dewald, D. Wachsmuth, J.-U. Grabow and S. C. Mehrotra, *J. Mol. Spectrosc.*, 2012, **280**, 54–60.

15 M. J. Frisch, G. W. Trucks, H. B. Schlegel, G. E. Scuseria, M. A. Robb, J. R. Cheeseman, G. Scalmani, V. Barone, B. Mennucci, G. A. Petersson, H. Nakatsuji, M. Caricato, X. Li, H. P. Hratchian, A. F. Izmaylov, J. Bloino, G. Zheng, J. L. Sonnenberg, M. Hada, M. Ehara, K. Toyota, R. Fukuda, J. Hasegawa, M. Ishida, T. Nakajima, Y. Honda, O. Kitao, H. Nakai, T. Vreven, J. A. Montgomery Jr., J. E. Peralta, F. Ogliaro, M. Bearpark, J. J. Heyd, E. Brothers, K. N. Kudin, V. N. Staroverov, R. Kobayashi, J. Normand, K. Raghavachari, A. Rendell, J. C. Burant, S. S. Iyengar, J. Tomasi, M. Cossi, N. Rega, J. M. Millam, M. Klene, J. E. Knox, J. B. Cross, V. Bakken, C. Adamo, J. Jaramillo, R. Gomperts, R. E. Stratmann, O. Yazyev, A. J. Austin, R. Cammi, C. Pomelli, J. W. Ochterski, R. L. Martin, K. Morokuma, V. G. Zakrzewski, G. A. Voth, P. Salvador, J. J. Dannenberg, S. Dapprich, A. D. Daniels, Ö. Farkas, J. B. Foresman, J. V. Ortiz, J. Cioslowski and D. J. Fox, *Gaussian 09 Revision E.01*, 2016, www.gaussian.com.

16 A. D. Becke, *Phys. Rev. A: At., Mol., Opt. Phys.*, 1988, **38**, 3098–3100.

17 C. Lee, W. Yang and R. G. Parr, *Phys. Rev. B: Condens. Matter Mater. Phys.*, 1988, **37**, 785–789.

18 A. D. Becke, *J. Chem. Phys.*, 1993, **98**, 1372–1377.

19 P. J. Stephens, F. J. Devlin, C. F. Chabalowski and M. J. Frisch, *J. Phys. Chem.*, 1994, **98**, 11623–11627.

20 S. Grimme, *J. Chem. Phys.*, 2006, **124**, 034108.

21 E. R. Johnson and A. D. Becke, *J. Chem. Phys.*, 2005, **123**, 024101.

22 S. Grimme, S. Ehrlich and L. Goerigk, *J. Comput. Chem.*, 2011, **32**, 1456–1465.

23 S. F. Boys and F. Bernardi, *Mol. Phys.*, 1970, **19**, 553–566.

24 D. E. Woon and T. H. Dunning, *J. Chem. Phys.*, 1993, **98**, 1358–1371.

This journal is © the Owner Societies 2020

Phys. Chem. Chem. Phys., 2020, **22**, 5615–5624 | **5623**

25 K. A. Peterson, D. Figgen, E. Goll, H. Stoll and M. Dolg, *J. Chem. Phys.*, 2003, **119**, 11099–11112.

26 K. A. Peterson and C. Puzzarini, *Theor. Chem. Acc.*, 2005, **114**, 283–296.

27 G. D. Purvis and R. J. Bartlett, *J. Chem. Phys.*, 1982, **76**, 1910–1918.

28 J. F. Stanton, J. Gauss, L. Cheng, M. E. Harding, D. A. Matthews and P. G. Szalay, CFOUR, Coupled-cluster techniques for computational chemistry, 2010, www.cfour.de.

29 R. M. Parrish, L. A. Burns, D. G. Smith, A. C. Simmonett, A. E. DePrince, E. G. Hohenstein, U. Bozkaya, A. Y. Sokolov, R. Di Remigio, R. M. Richard, J. F. Gonthier, A. M. James, H. R. McAlexander, A. Kumar, M. Saitow, X. Wang, B. P. Pritchard, P. Verma, H. F. Schaefer, K. Patkowski, R. A. King, E. F. Valeev, F. A. Evangelista, J. M. Turney, T. D. Crawford and C. D. Sherrill, *J. Chem. Theory Comput.*, 2017, **13**, 3185–3197.

30 T. M. Parker, L. A. Burns, R. M. Parrish, A. G. Ryno and C. D. Sherrill, *J. Chem. Phys.*, 2014, **140**, 094106.

31 K. A. Peterson and T. H. Dunning, *J. Chem. Phys.*, 2002, **117**, 10548–10560.

32 A. Halkier, T. Helgaker, P. Jørgensen, W. Klopper and J. Olsen, *Chem. Phys. Lett.*, 1999, **302**, 437–446.

33 A. Wolf, M. Reiher and B. A. Hess, *J. Chem. Phys.*, 2002, **117**, 9215–9226.

34 C. T. Campos and F. E. Jorge, *Mol. Phys.*, 2013, **111**, 165–171.

35 Z. Kisiel, *J. Mol. Spectrosc.*, 2003, **218**, 58–67.

36 Z. Kisiel, PROSPE – Programs for rotational spectroscopy, Accessed: 2019-03-19, http://info.ifpan.edu.pl/~kisiel/prospe.htm.

37 V. Barone, *J. Chem. Phys.*, 2005, **122**, 014108.

38 P. Schwerdtfeger and J. K. Nagle, *Mol. Phys.*, 2019, **117**, 1200–1225.

39 B. Jeziorski, R. Moszynski and K. Szalewicz, *Chem. Rev.*, 1994, **94**, 1887–1930.

40 C. R. Jacob, T. A. Wesolowski and L. Visscher, *J. Chem. Phys.*, 2005, **123**, 174104.

41 H. Zhu, Y. Guo, Y. Xue and D. Xie, *J. Comput. Chem.*, 2006, **27**, 1045–1053.

42 J. M. Howson and J. M. Hutson, *J. Chem. Phys.*, 2001, **115**, 5059–5065.

43 E. Feng, C. Sun, C. Yu, X. Shao and W. Huang, *J. Chem. Phys.*, 2011, **135**, 124301.

44 D. J. Millen, *Can. J. Chem.*, 1985, **63**, 1477–1479.

45 J. K. G. Watson, in *Vibrational spectra and structure*, ed. J. R. Durig, Elsevier, 1977.

46 M. O. Sinnokrot and C. D. Sherrill, *J. Chem. Phys.*, 2001, **115**, 2439–2448.

47 W. X. Pang, H. Y. Wu, J. J. Zhao and Y. B. Sun, *Phosphorus, Sulfur Silicon Relat. Elem.*, 2019, **194**, 69–75.

48 P. Kraus and I. Frank, *J. Phys. Chem. A*, 2018, **122**, 4894–4901.

49 J. K. G. Watson, A. Roytburg and W. Ulrich, *J. Mol. Spectrosc.*, 1999, **196**, 102–119.

50 J. K. G. Watson, *J. Mol. Spectrosc.*, 2001, **207**, 16–24.

51 A. J. Varandas, *Annu. Rev. Phys. Chem.*, 2018, **69**, 177–203.

52 J. Řezáč and P. Hobza, *J. Chem. Theory Comput.*, 2013, **9**, 2151–2155.

53 P. Kraus and I. Frank, *Int. J. Quantum Chem.*, 2019, **119**, e25953.

54 D. A. Obenchain, L. Spada, S. Alessandrini, S. Rampino, S. Herbers, N. Tasinato, M. Mendolicchio, P. Kraus, J. Gauss, C. Puzzarini, J.-U. Grabow and V. Barone, *Angew. Chem., Int. Ed.*, 2018, **57**, 15822–15826.

5624 | *Phys. Chem. Chem. Phys.*, 2020, **22**, 5615–5624

This journal is © the Owner Societies 2020